Chapter

Power System Small-Signal Stability as Affected by Grid-Connected SmartPark

Cai Hui

Abstract

Large-scale smart charging stations can effectively satisfy and control the charging demands of tremendous plug-in electric vehicles (PEVs). But, simultaneously, their penetrations inevitably induce new challenges to the operation of power systems. In this chapter, damping torque analysis (DTA) was employed to examine the effects of the integration of smart charging station on the dynamic stability of the transmission system. A single-machine infinite-bus power system with a smart charging station that denoted the equivalent of several ones was used for analysis. The results obtained from DTA reveal that in view of the damping ratio, the optimal charging capacity is better to be considered in the design of the smart charging station. Under the proposed charging capacity, the power system can achieve the best maintained dynamic stability, and the damping ratio can reach the crest value. Phase compensation method was utilized to design the stabilizer via the active and reactive power regulators of the smart charging station respectively. With the help of the stabilizers, damping of the system oscillation under certain operating conditions can be significantly improved, and the power oscillation in the tie-line can be suppressed more quickly.

Keywords: smart charging station, plug-in electric vehicles (PEVs), power system oscillations, small-signal stability, damping torque analysis (DTA), stabilizer design

1. Introduction

The growing concern of carbon dioxide emission, greenhouse effect, and rapid depletion of fossil energy drives the demand for the revolutionary changes in the automobile industry. Much effort has been put into developing a new high-efficient, environment-friendly, and safe transportation vehicle that can replace the conventional ones. The utilization of plug-in electric vehicles (PEVs) as the most suitable solution has been promoted in many countries. China is expected to have 5 million electric vehicles (EVs) by 2020 according to its Development Plan for Energy-saving and Renewable Energy Vehicles. However, a prediction by State Grid Corporation of China (SGCC) illustrates that the number will be 5–10 million due to the fast development of EVs at present in China. As EV-related technologies have been making progress and many national and local incentives have been created for EV purchases, the total number of EVs is likely to be 30 million by 2030 [1–3].

With the significant increase of PEVs, the corresponding parking lots termed as smart charging stations in [4–8] will be established to charge the tremendous PEVs. A typical city will contain several SmartParks, as the aggregator of numerous EV charging stations, distributed throughout the city one to few miles apart in the distribution system. The newly established smart charging stations are preferred to be connected to an additional bus of the transmission system [3–5]. The vehicle-to-grid (V2G) technology supplies the bidirectional communication between the parked vehicles and connected grid. The vehicles parked in the smart charging station can not only simply absorb active power (AP) from the grid for charging, but also participate in power regulation during discharging mode. Ref. [7] shows that most personal vehicles in the U.S. were parked more than 95% of the day and generally followed a daily schedule. The huge number of parked PEVs has the assignable potential to impact the frequency stability, voltage stability, and rotor-angle stability of the system [9–16]. Nowadays, the capacity of smart charging stations is much lower than that of the conventional power plants. Only frequency stability and voltage stability of the distribution systems attract much attention in recent years. However, if only half of the 230 million gasoline-powered cars, sport utility vehicles, and light trucks in U.S. are converted to or replaced with the electric vehicles, they would have 20 times the power capacity of all electricity in the country [17]. The impacts of SmartParks on the stability of the transmission systems cannot be ignored any more. Power system oscillations, as one section of the dynamic stability, occur inherently due to the rotor inertia of synchronous generators such that it takes time for them to respond to the sudden lack or excess of active power in a power system. The increased amplitude or weakly damped power oscillations via the tie-lines will lead to wrong activation of the automatic protection devices, splitting of the system, or even collapse. While the time-varying nature of the load-flow condition in the power system with high-penetrated smart charging stations is the common reason for the appearance of power oscillations, damping torque of the system is extremely interesting.

Under different operating conditions, smart charging stations can vary from the adjustable load in the charging mode to the regulable generator in the discharging mode and vice versa with the voltage control strategy [4–6]. It is significantly valuable to examine how and why it may interact with the conventional power generation, hence affecting power system small-signal stability. In order to gain a good understanding on and clear insight into this interaction through theoretical analysis, a single-machine infinite-bus power system is adopted in this chapter. A smart charging station is connected to the system and theoretical damping torque analysis is carried out to check how and why the smart charging station interacts with the single generator so as to affect the power oscillation. It is expected that the analytical conclusions obtained in the chapter can be used to guide further work on a more complicated case of the oscillations in multi-machine power systems.

The organization of this chapter is as follows: in Section 2, a comprehensive model of a single-machine infinite-bus power system integrated with a smart charging station is established. After that, damping torque analysis (DTA) [18–21] is employed to examine the effect of joint operation of a smart charging station and a conventional synchronous machine on the system's small-signal stability in Section 3. The result of the damping torque analysis indicates that the smart charging station does not contribute an extra mode of electromechanical oscillation. It affects power system small-signal stability by supplying either positive or negative damping torque to the conventional power plant varying with the system operating conditions. Analysis also reveals that from the view of damping ratio,

the optimal charging capacity is better to be considered during the design of the smart charging station. In Section 4, the phase compensation method is utilized to design the stabilizer via the active power and reactive power (RP) regulators of the smart charging station, respectively. A single-machine infinite-bus power system integrated with a smart charging station is presented as an example in Section 5. Results of numerical computation, non-linear simulations, and eigenvalue calculations at different system operating conditions are given. These simulations and results demonstrate and confirm the presented theoretical analysis, and verify the effectiveness of the designed stabilizer. Another four-machine power system is employed to show that the conclusions obtained in the single-machine power system are also available in the multi-machine power system. Conclusions are summarized in Section 6.

2. A linearized model of single-machine infinite-bus system with a smart charging station

The local electricity generation systems, besides supporting the regional loads, can be used to charge a smart charging station under usual conditions. Comparing with 1000-million-kilowatt capacity of outer power systems, the abundant active power generation with 10,000-kilowatt capacity in a regional system can be simplified as an equivalent synchronous machine. The inertia of the equivalent synchronous machine denotes the dynamic stability of the regional system. Because every individual smart charging station has the same dynamic behavior during the transient procedure, the smart charging stations can be regarded as an equivalent one with higher active power and reactive power capacities. A smart charging station usually is connected to the transmission system through a step-up transformer, which is seen as a reactance in this chapter.

In this chapter, the research focuses on the power oscillation which lasts for mostly 10–20 s. Uncertainties during EV charging such as the alternations of charging strategies or vehicle numbers have little effect on this analysis. EV charging demand or discharging supply during this dynamic procedure is considered as determinate power from the start time and following seconds. For a simple analysis, a constant power charging/discharging strategy is utilized to estimate the optimal EV charging numbers for smart charging station design.

Figure 1 shows the configuration of a single-machine infinite-bus power system, where a smart charging station is connected at a busbar denoted by subscript s. The linearized models of network equations and synchronous machine are presented in [18, 22, 23].

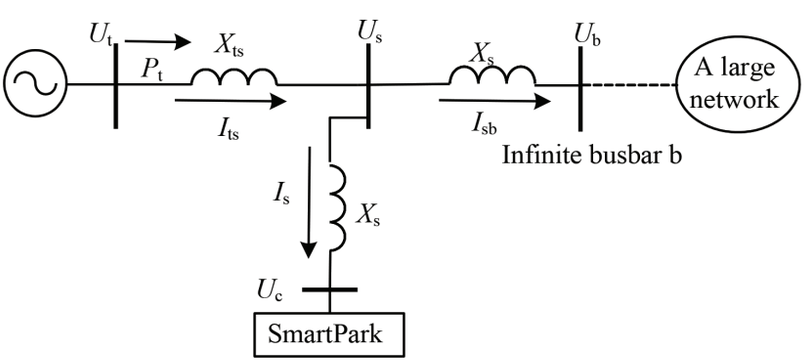

Figure 1.
Simplified model of the power system in a city.

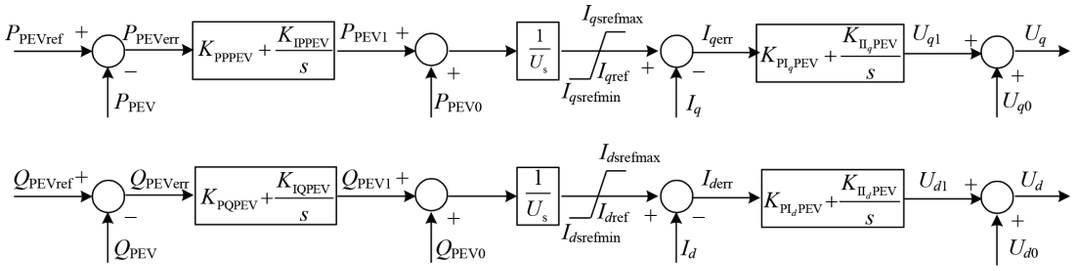

Figure 2.
Control strategy of a smart charging station.

Here, U_s is the voltage at the high-voltage-level busbar where the smart charging station locates; U_b and U_c are the voltages at infinite busbar and the low-voltage-level busbar connected with the smart charging station; I_{ts}, I_s, and I_{sb} are the line currents as indicated in **Figure 1**; and X_{ts}, X_{sb}, and X_s are line reactances as indicated in **Figure 1**.

The control strategy of smart charging stations is shown in **Figure 2**.

The objective control is to command the currents corresponding to the fast change in demanded active and reactive power. The equations of smart charging stations according to **Figure 2** are obtained as:

$$\begin{cases} \begin{cases} P_1 = (K_{PP} + K_{IP}/s)(P_{PEVref} - P_{PEV}) \\ I_{qsref} = \dfrac{P_1 + P_{10}}{U_s} \\ U_{qc1} = \left(K_{PI_q} + K_{II_q}/s\right)\left(I_{qsref} - I_{qs}\right) \\ U_{qc} = U_{qc0} + U_{qc1} \end{cases} \\ \begin{cases} Q_1 = \left(K_{PQ} + K_{IQ}/s\right)(Q_{PEVref} - Q_{PEV}) \\ I_{dsref} = \dfrac{Q_1 + Q_{10}}{U_s} \\ U_{dc1} = \left(K_{PI_d} + K_{II_d}/s\right)(I_{dsref} - I_{ds}) \\ U_{dc} = U_{dc0} + U_{dc1} \end{cases} \end{cases} \tag{1}$$

where

P_{PEV} and Q_{PEV} are the demanded active and reactive power by the smart charging station and

$K_{PP} + \frac{K_{IP}}{s}$, $K_{PQ} + \frac{K_{IQ}}{s}$, $K_{PI_d} + \frac{K_{II_d}}{s}$, $K_{PI_q} + \frac{K_{II_q}}{s}$ are the proportional-integral controllers in the smart charging station.

Linearized from Eq. (1),

$$\begin{cases} \Delta U_{dc} = K_{U_{dc}U_{dc}}\Delta U_{dc} + K_{U_{dc}U_{qc}}\Delta U_{qc} + K_{U_{dc}E_q'}\Delta E_q' + K_{U_{dc}\delta}\Delta\delta \\ \Delta U_{qc} = K_{U_{qc}U_{dc}}\Delta U_{dc} + K_{U_{qc}U_{qc}}\Delta U_{qc} + K_{U_{qc}E_q'}\Delta E_q' + K_{U_{qc}\delta}\Delta\delta \end{cases} \tag{2}$$

where

$$\begin{cases} \Delta P_{PEV} = K_{PPU_{dc}}\Delta U_{dc} + K_{PPU_{qc}}\Delta U_{qc} + K_{PPE_q'}\Delta E_q' + K_{PP\delta}\Delta\delta \\ \Delta Q_{PEV} = K_{QPU_{dc}}\Delta U_{dc} + K_{QPU_{qc}}\Delta U_{qc} + K_{QPE_q'}\Delta E_q' + K_{QP\delta}\Delta\delta \\ \Delta U_s = K_{U_sU_{dc}}\Delta U_{dc} + K_{U_sU_{qc}}\Delta U_{qc} + K_{U_sE_q'}\Delta E_q' + K_{U_s\delta}\Delta\delta \end{cases} \tag{3}$$

Arranging from Eq. (2),

$$\begin{cases} \Delta U_{dc} = K_{\text{sp-U}_{dc}\text{E}_q'} \Delta E_q' + K_{\text{sp-U}_{dc}\delta} \Delta\delta \\ \Delta U_{qc} = K_{\text{sp-U}_{qc}\text{E}_q'} \Delta E_q' + K_{\text{sp-U}_{qc}\delta} \Delta\delta \end{cases} \tag{4}$$

While this chapter focuses on the analysis of the impact from the grid-connected smart charging station to the system small-signal stability, linearized processes and expressions for coefficients are not specifically listed.

3. Analysis of damping torque contribution from the Phillips-Heffron model

The Phillips-Heffron model of a smart charging station, which is based on the linearization of the system and describes the relationships between all variables, assessed to the single-machine infinite-busbar (SMIB) power system can be obtained as **Figure 3**, where the Phillips-Heffron model of SMIB only is referred to Refs. [22–24]. From Eqs. (2) and (3), the model of the smart charging station and its control strategy can be obtained as **Figure 4**.

From **Figures 3** and **4**, we have:

$$\begin{aligned} \Delta T_{\text{et-sp}} &= \Delta T_{\text{st-sp}} + j\Delta T_{\text{dt-sp}} = K_{\text{PU}_{dc}} \Delta U_{dc} + K_{\text{PU}_{qc}} \Delta U_{qc} \\ &= \left(K_{\text{PU}_{dc}} K_{\text{sp-U}_{dc}\delta} + K_{\text{PU}_{qc}} K_{\text{sp-U}_{qc}\delta} \right) \Delta\delta \end{aligned} \tag{5}$$

$$\begin{aligned} \Delta T_{\text{et-ex}} &= \Delta T_{\text{st-ex}} + j\Delta T_{\text{dt-ex}} = K_{\text{PE}_q'} \\ &\quad - \left[K_{\text{E}_q\text{U}_{qc}} K_{\text{sp-U}_{qc}\delta} + K_{\text{E}_q\delta} - \frac{K_a}{1+sT_a} \left(K_{\text{U}_t\text{U}_{dc}} K_{\text{sp-U}_{dc}\delta} + K_{\text{U}_t\text{U}_{qc}} K_{\text{sp-U}_{qc}\delta} + K_{\text{U}_t\delta} \right) \right] \\ &\quad \overline{\left(T_{d0}' s + K_{\text{E}_q\text{E}_q'} \right) + K_{\text{E}_q\text{U}_{qc}} K_{\text{sp-U}_{qc}\text{E}_q'} - \frac{K_a}{1+sT_a} \left(K_{\text{U}_t\text{U}_{dc}} K_{\text{sp-U}_{dc}\text{E}_q'} + K_{\text{U}_t\text{U}_{qc}} K_{\text{sp-U}_{qc}\text{E}_q'} + K_{\text{U}_t\text{E}_q'} \right)} \Delta\delta \end{aligned} \tag{6}$$

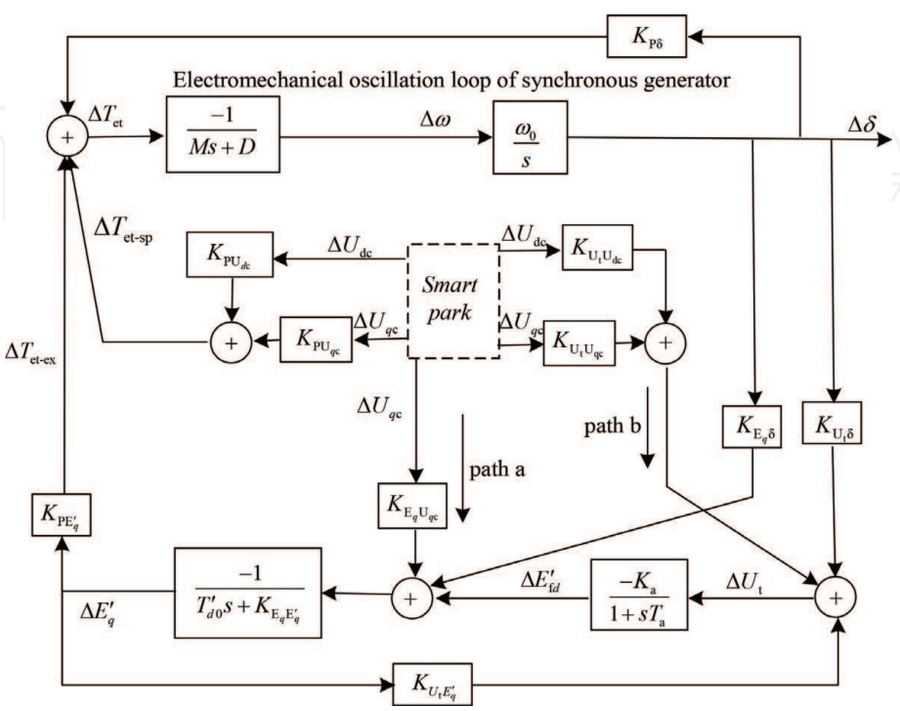

Figure 3.
Phillips-Heffron model of the single-machine infinite-busbar system with a smart charging station.

$$\Delta T_{et} = \Delta T_{st} + j\Delta T_{dt} = \Delta T_{et\text{-}sp} + \Delta T_{et\text{-}ex} = \left(\Delta T_{st\text{-}sp} + \Delta T_{st\text{-}ex}\right) + j\left(\Delta T_{dt\text{-}sp} + \Delta T_{dt\text{-}ex}\right) \tag{7}$$

Figures 3 and **4** clearly show the dynamic interaction between the smart charging station and the conventional synchronous generator. **Figure 3** is very similar to the conventional Phillips-Heffron model based on which the DTA was proposed and developed. It shows that the smart charging station interacts closely with the generator by contributing the electric torque to the electromechanical oscillation loop of the generator. The contribution of electric torque is comprised of two parts, viz. $\Delta T_{et\text{-}sp}$ which relates to $\Delta\delta$ and directly affects the oscillation loop, and $\Delta T_{et\text{-}ex}$ which relates to $\Delta E'_q$ and functions through the excitation system, as indicated in **Figure 3**. According to DTA, the electric torque can be decomposed into two components, viz. the synchronizing torque and the damping torque as shown in Eq. (7). The damping torque contributions $\Delta T_{dt\text{-}sp}$, $\Delta T_{dt\text{-}ex,}$ and ΔT_{dt} determine the influences on the damping of power system oscillation.

With certain output power of the synchronous machine and absorbed or injected power of the smart charging station, the bus voltages and currents of the corresponding operation condition can be determined. The damping torques $\Delta T_{dt\text{-}sp}$,

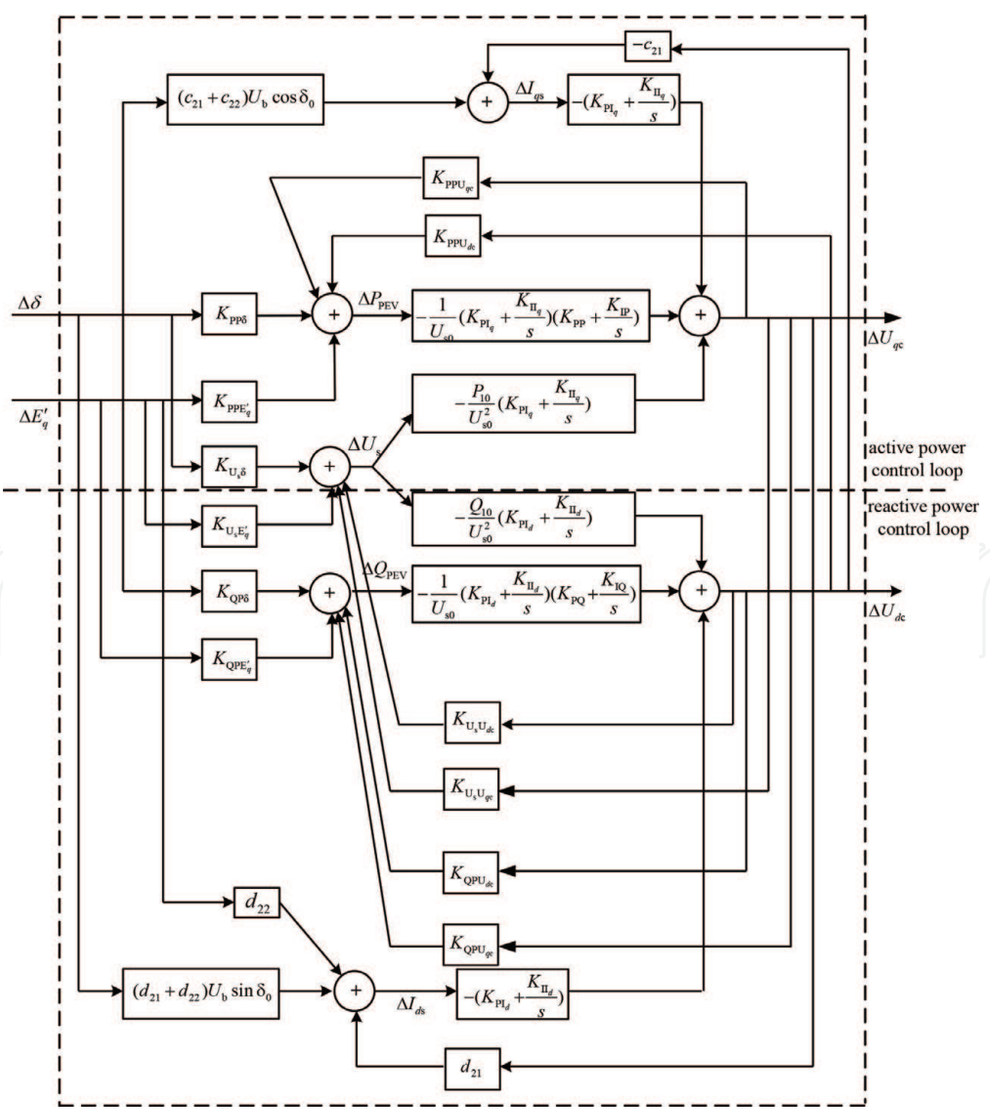

Figure 4.
Linearized model of a smart charging station and its control.

$\Delta T_{\text{dt-ex}}$, and ΔT_{dt} are dependent on the output power of the synchronous machine and the absorbed or injected power of the smart charging station.

From Eqs. (5)–(7), the conclusions can be summarized as follows:

1. The proportional controls K_{p} in the smart charging station mainly induce the synchronous torque into the oscillation loop, while for $\Delta T_{\text{et-sp}}$ in Eq. (5), only its real part is related to $\Delta\delta$; and the majority of damping torque is introduced by integral controls K_{i}/s, because $1/s$ induces the imaginary part in $\Delta T_{\text{et-sp}}$ relating to $\Delta\omega$.

2. Because the signals ΔU_{dc} and ΔU_{qc} through path a and path b in **Figure 3** are significantly attenuated by lag loops before they form one part of the damping torque through the excitation system [24], the damping torque contribution from them can be neglected for simplified analysis. $\Delta T_{\text{dt-sp}}$ represents the main damping torque supplied by the smart charging station in damping torque analysis, and $\Delta T_{\text{dt-ex}}$ mainly expresses the torque supplied by the excitation system of the synchronous machine.

3. In this chapter, the '−' sign indicates the vehicles are selling power to the grid, that is, they are in discharging mode and the '+' sign indicates that they are buying power from the gird, denoting that the vehicles are in charging mode.

The optimal operation point when the system has the biggest damping torque can be calculated as:

$$\frac{\partial \Delta T_{\text{dt}}}{\partial P_{\text{PEV}}} = \frac{\partial \Delta T_{\text{dt-sp}} + \partial \Delta T_{\text{dt-ex}}}{\partial P_{\text{PEV}}} = 0 \& \frac{\partial^2 \Delta T_{\text{dt}}}{\partial P_{\text{PEV}}^2} \leq 0 \ \text{ when } P_{\text{PEV}} > 0 \tag{8}$$

When the output power of the synchronous machine is fixed, the positive or negative damping torque supplied by the excitation system of the synchronous machine is only slightly changed. At the optimal operation point, the total damping torque ΔT_{dt} of the system and $\Delta T_{\text{dt-sp}}$ contributed from the smart charging station both reach their maximum values.

When the active power in the tie-line is fixed, the output power of the synchronous machine is changed corresponding to the absorbed or injected power of the smart charging station. Both damping torques contributed by the smart charging station and the excitation system need to be considered. The total damping torque ΔT_{dt} of the system and $\Delta T_{\text{dt-sp}}$ contributed from the smart charging station reach their maximum values at different operation points.

4. Design for the stabilizer attached to the smart charging station

Under the operation conditions that the total damping torques supplied by the smart charging station and the excitation system are not enough to suppress the oscillations, additional damping torques need to be added. Compared with the installation and coordinated parameter setting for power system stabilizers (PSSs) in synchronous machines, smart charging stations can be simply utilized to suppress the grid's active power oscillation with little infrastructure cost. Only a centralized stabilizer will be required at the smart charging station to maintain system stability.

The stabilizer added via the active power (AP) or reactive power (RP) control loop is shown in **Figure 5**.

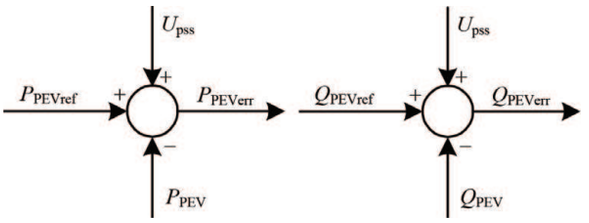

Figure 5.
Control strategy of the stabilizer added via AP and RP control loop, respectively.

The forward path function which describes the way from output signal of the stabilizer to the additional damping torque into the electromechanical oscillation loop can be obtained:

$$\begin{cases} F_{\mathrm{pssp}}(s) = \dfrac{\partial \Delta T_{\mathrm{pss}}}{\partial \Delta u_{\mathrm{pssp}}} = K_{\mathrm{PU}_{dc}} K_{\mathrm{sp\text{-}U}_{dc}\mathrm{u}_{\mathrm{pssp}}} + K_{\mathrm{PU}_{qc}} K_{\mathrm{sp\text{-}U}_{qc}\mathrm{u}_{\mathrm{pssp}}} + \\ \qquad K_{\mathrm{PE}'_q} \dfrac{-\left[K_{\mathrm{E}_q\mathrm{U}_{qc}} K_{\mathrm{sp\text{-}U}_{qc}\mathrm{u}_{\mathrm{pssp}}} - \dfrac{K_{\mathrm{a}}}{1+sT_{\mathrm{a}}}\left(K_{\mathrm{U_tU}_{dc}} K_{\mathrm{sp\text{-}U}_{dc}\mathrm{u}_{\mathrm{pssp}}} + K_{\mathrm{U_tU}_{qc}} K_{\mathrm{sp\text{-}U}_{qc}\mathrm{u}_{\mathrm{pssp}}}\right)\right]}{\left(T'_{d0}s + K_{\mathrm{E}_q\mathrm{E}'_q}\right) + K_{\mathrm{E}_q\mathrm{U}_{qc}} K_{\mathrm{sp\text{-}U}_{qc}\mathrm{E}'_q} - \dfrac{K_{\mathrm{a}}}{1+sT_{\mathrm{a}}}\left(K_{\mathrm{U_tU}_{dc}} K_{\mathrm{sp\text{-}U}_{dc}\mathrm{E}'_q} + K_{\mathrm{U_tU}_{qc}} K_{\mathrm{sp\text{-}U}_{qc}\mathrm{E}'_q} + K_{\mathrm{U_tE}'_q}\right)} \\ F_{\mathrm{pssq}}(s) = \dfrac{\partial \Delta T_{\mathrm{pss}}}{\partial \Delta u_{\mathrm{pssq}}} = K_{\mathrm{PU}_{dc}} K_{\mathrm{sp\text{-}U}_{dc}\mathrm{u}_{\mathrm{pssq}}} + K_{\mathrm{PU}_{qc}} K_{\mathrm{sp\text{-}U}_{qc}\mathrm{u}_{\mathrm{pssq}}} + K_{\mathrm{PE}'_q} \\ \qquad \dfrac{-\left[K_{\mathrm{E}_q\mathrm{U}_{qc}} K_{\mathrm{sp\text{-}U}_{qc}\mathrm{u}_{\mathrm{pssq}}} - \dfrac{K_{\mathrm{a}}}{1+sT_{\mathrm{a}}}\left(K_{\mathrm{U_tU}_{dc}} K_{\mathrm{sp\text{-}U}_{dc}\mathrm{u}_{\mathrm{pssq}}} + K_{\mathrm{U_tU}_{qc}} K_{\mathrm{sp\text{-}U}_{qc}\mathrm{u}_{\mathrm{pssq}}}\right)\right]}{\left(T'_{d0}s + K_{\mathrm{E}_q\mathrm{E}'_q}\right) + K_{\mathrm{E}_q\mathrm{U}_{qc}} K_{\mathrm{sp\text{-}U}_{qc}\mathrm{E}'_q} - \dfrac{K_{\mathrm{a}}}{1+sT_{\mathrm{a}}}\left(K_{\mathrm{U_tU}_{dc}} K_{\mathrm{sp\text{-}U}_{dc}\mathrm{E}'_q} + K_{\mathrm{U_tU}_{qc}} K_{\mathrm{sp\text{-}U}_{qc}\mathrm{E}'_q} + K_{\mathrm{U_tE}'_q}\right)} \end{cases} \tag{9}$$

where,

F_{pssp} or F_{pssq} is corresponding to the utilized output signal of the stabilizer u_{pssp} or u_{pssq}.

$K_{\mathrm{sp\text{-}U}_{dc}\mathrm{u}_{\mathrm{pssp}}}$, $K_{\mathrm{sp\text{-}U}_{qc}\mathrm{u}_{\mathrm{pssp}}}$, $K_{\mathrm{sp\text{-}U}_{dc}\mathrm{u}_{\mathrm{pssq}}}$ and $K_{\mathrm{sp\text{-}U}_{qc}\mathrm{u}_{\mathrm{pssq}}}$ are obtained from the linearization of the control strategy with the output signals of the stabilizer considered.

The active power P_{b} in the tie-line is chosen for the feedback signals of the stabilizers via the active power regulator and the reactive power regulator.

From the linear system control theory, the active power P_{b} can be written as a function of the rotor speed of the generator.

$$\Delta P_{\mathrm{b}} = r_{\mathrm{P}}(s)\Delta\omega \tag{10}$$

where $r_{\mathrm{P}}(s) = \left(K_{\mathrm{P_b}\delta} + K_{\mathrm{P_bE}'_q} K_{\mathrm{E}'_q\delta}\right)\frac{\omega_0}{s}$ is the reconstruction function for P_{b}.

While $\Delta P_{\mathrm{b}} = \Delta P_{\mathrm{t}} - \Delta P_{\mathrm{PEV}}$, $K_{\mathrm{P_b}\delta}$, $K_{\mathrm{P_bE}'_q}$ and $K_{\mathrm{E}'_q\delta}$ are related to the reconstruction of this feedback signal.

Considering Eqs. (9) and (10), the electric torques contributed by the stabilizer via active and reactive power regulators, respectively, are expressed as:

$$\begin{cases} \Delta\mathbf{T}\left(\Delta u_{\mathrm{pssp}}\right) = F_{\mathrm{pssp}}(s) r_{\mathrm{p}}(s) G_{\mathrm{PEVP}}(s)\Delta\omega \\ \Delta\mathbf{T}\left(\Delta u_{\mathrm{pssq}}\right) = F_{\mathrm{pssq}}(s) r_{\mathrm{p}}(s) G_{\mathrm{PEVQ}}(s)\Delta\omega \end{cases} \tag{11}$$

where $G_{\mathrm{PEVP}}(s)$ and $G_{\mathrm{PEVQ}}(s)$ are the transfer function of the stabilizer via active and reactive power regulators respectively.

The transfer function of the stabilizer is

$$G_{\mathrm{PEV}} = K_{\mathrm{w}} \frac{1+sT_2}{1+sT_1} \frac{1+sT_4}{1+sT_3} \tag{12}$$

The stabilizers are designed to compensate the lagging or leading angle of the forward path, in order to supply maximum positive damping into the system. The phase compensation method is used to design the parameters of the stabilizers.

5. Case study

5.1 Case description

Two example cases are employed in this section. From Case A to Case D, a single-machine infinite-busbar power system is used. The parameters of the system are given in Appendix A.1. Under different capacities of the smart charging station, computational results of the damping torque contribution from the smart charging station and the excitation system to the electromechanical oscillation loop of the single synchronous generator are obtained and confirmed by the eigenvalue of the system's oscillation mode. The critical point in which the system has the biggest damping torque is highlighted. In Case E, a four-machine power system is presented. The parameters are given in Appendix A.2. The eigenvalue related to the inter-area oscillation mode is concerned under different capacities of the smart charging station.

5.2 Case A: utilizing only proportional control in the smart charging station and fixing load-flow in the tie-line

With the load-flow in the tie-line fixed at 10 MW, the comparison is done when only proportional control is utilized in the smart charging station under its different charging or discharging power capacities. The computational results of the example system are shown in **Table 1**, when only P control is utilized in the smart charging station. From **Table 1**, it can be concluded that:

P_{t}/(10 MW)	P_{PEV}/(10 MW)	ΔT_{dt}/pu	$\Delta T_{\mathrm{dt\text{-}sp}}$/pu	$\Delta T_{\mathrm{dt\text{-}ex}}$/pu	Frequency/Hz	Damping ratio/%
4.0	3.0	0.6340	0.0006	0.6334	1.83	3.19
3.5	2.5	0.7842	0.0004	0.7838	1.82	3.47
3.0	2.0	0.4368	0.0002	0.4366	1.74	2.99
2.5	1.5	−0.1877	−0.0003	−0.1874	1.68	1.92
2.0	1.0	−0.5730	−0.0005	−0.5725	1.61	1.24
1.5	0.5	−0.1870	−0.0002	−0.1868	1.68	1.92
1.0	0.0	0.4345	0.0003	0.4342	1.74	2.99
0.5	−0.5	0.7851	0.0005	0.7846	1.82	3.47
0.0	−1.0	0.6348	0.0007	0.6341	1.83	3.19

Table 1.
Computational results of the example system when only P control is utilized in the smart charging station.

1. The total damping torque contribution ΔT_{dt} is approximately equal to the damping torque from the excitation system $\Delta T_{dt\text{-}ex}$. The change of ΔT_{dt} is mainly induced by $\Delta T_{dt\text{-}ex}$ which is the impact from the excitation system of the synchronous machine under different output power. The smart charging station only with the proportional control functions as an adjustable load in charging mode or as a regulator generator in discharging mode.

2. Integral control in the smart charging station not only helps to reduce the steady-state error and accelerate the smart charging station to the steady operation point, but also supplies either positive or negative damping torque into the system. It demonstrates conclusion (1) obtained in Section 3.

5.3 Case B: utilizing PI control in the smart charging station and fixing output power of the synchronous machine

A comparison of the damping torques is made under different charging or discharging power capacities of the smart charging station with the fixed output power of the synchronous machine. The computational results of the example system are shown in **Table 2**, when active power supplied by the synchronous machine is fixed at 10 MW. From **Table 2**, it can be concluded that:

1. While the output of the synchronous machine is constant, the damping torque from the excitation system of the synchronous machine is nearly unchanged. The signals ΔU_{dc} and ΔU_{qc} through path a and path b only contribute slight changes to $\Delta T_{dt\text{-}ex}$. The variety of total damping torque contribution ΔT_{dt} is mainly induced from $\Delta T_{dt\text{-}sp}$ which comes from the smart charging station and directly affects the oscillation loop. It demonstrates conclusion (2) obtained in Section 3.

2. The damping torque from the smart charging station changes at its different charging or discharging capacity, which is either positive or negative. The smart charging station can help to improve the damping with certain charging capacity which is between the lower and upper threshold. In charging mode, the smart charging station is preferred to operate around 10 MW which is nearly the same as 10.4 MW calculated by Eq. (8). The highest total damping

P_t/(10 MW)	P_{PEV}/(10 MW)	ΔT_{dt}/pu	$\Delta T_{dt\text{-}sp}$/pu	$\Delta T_{dt\text{-}ex}$/pu	Frequency/Hz	Damping ratio/%
1.0	3.0	0.0633	−0.3182	0.3815	1.69	2.38
1.0	2.5	0.1560	−0.2452	0.4021	1.72	2.51
1.0	2.0	0.3742	−0.0457	0.4199	1.74	2.88
1.0	1.5	0.8400	0.3798	0.4602	1.75	3.71
1.0	1.0	1.0677	0.5806	0.4871	1.76	4.10
1.0	0.5	0.8180	0.3699	0.4481	1.75	3.67
1.0	0.0	0.3523	−0.0582	0.4105	1.74	2.84
1.0	−0.5	0.1398	−0.2593	0.3991	1.72	2.48
1.0	−1.0	0.0227	−0.3370	0.3597	1.70	2.29

Table 2.
Computational results of the example system when active power supplied by the synchronous machine is fixed at 10 MW.

torque and damping torque from the smart charging station coincided at the same point. It demonstrates conclusion (3) obtained in Section 3. Under this operation point, the smart charging station just consumes the electricity generated by the equivalent synchronous machine. There is no active power exchange in the tie-line. Beyond or below this point, the damping ratio of the system will decrease because of the increased load burden in the tie-line either from the synchronous machine to the infinite bus or vice versa. Considering each vehicle can draw ±3.5 kW of active power [25] and always around 60% personal vehicles in the parking lots need to be charged [26], roughly 5000 personal vehicles are optimal to be accepted in this equivalent smart charging station.

3. During the discharging process, the damping of the system tends to deteriorate with the increasing power injected from the smart charging station to grid.

5.4 Case C: utilizing PI control in the smart charging station and fixing load-flow in the tie-line

A comparison of the damping torques is made under different charging or discharging power capacities of the smart charging station with the fixed load-flow in the tie-line. The results are shown in **Table 3**.

From **Table 3**, it can be concluded that:

1. The total damping torque contribution ΔT_{dt} is simultaneously influenced by $\Delta T_{\mathrm{dt\text{-}sp}}$ which relates to $\Delta\delta$ and directly affects the oscillation loop, and $\Delta T_{\mathrm{dt\text{-}ex}}$ which relates to $\Delta E'_q$ and functions through the excitation system.

2. The damping torque supplied from the smart charging station and the excitation system of the synchronous machine respectively is complementary during the charging process. Compared with **Table 1**, the positive damping torque supplied by the smart charging station helps the system to improve the low damping capacity from 5 to 15 MW in charging mode of the smart charging station. This conclusion can be confirmed by the analysis from Eqs. (5) and (6). When the charging power of the smart charging station is between 0 and 30 MW, the product of $\Delta T_{\mathrm{dt\text{-}sp}}$ and $\Delta T_{\mathrm{dt\text{-}ex}}$ is negative.

P_t/ (10 MW)	P_{PEV}/ (10 MW)	ΔT_{dt}/pu	$\Delta T_{dt\text{-}sp}$/pu	$\Delta T_{dt\text{-}ex}$/pu	Frequency/ Hz	Damping ratio/%
4.0	3.0	0.3144	−0.2878	0.6022	1.72	2.80
3.5	2.5	0.5527	−0.2122	0.7649	1.72	3.24
3.0	2.0	0.3902	−0.0082	0.3984	1.72	2.94
2.5	1.5	0.1770	0.3152	−0.1382	1.73	2.53
2.0	1.0	0.0093	0.5294	−0.5201	1.73	2.22
1.5	0.5	0.1693	0.3122	−0.1429	1.73	2.52
1.0	0.0	0.3523	−0.0582	0.4105	1.74	2.84
0.5	−0.5	0.5062	−0.2091	0.7153	1.73	3.14
0.0	−1.0	0.2971	−0.2908	0.5879	1.73	2.75

Table 3.
Computational results of the example system when load-flow in the tie-line is fixed at 10 MW.

3. The impact of the damping torque from the synchronous machine also needs to be considered. With this impact, the highest total damping torque and damping torque from the smart charging station are obtained at different points. In this case, the optimized operation point reaches 25 MW which is nearly the same as 24.6 MW calculated by Eq. (8). It demonstrates conclusion (3) in Section 3. Under the operating conditions that the absorbed power of the smart charging station varies from 20 to 25 MW, although the smart charging station supplies the negative damping torque into the grid, the total damping torque is still positive and keeps increasing with the compensation of the damping torque from the excitation system. The smart charging station at the optimal operation point is also charged by the electricity generated by the equivalent local synchronous machine.

4. The damping of the system tends to deteriorate with the increasing power injected from the smart charging station to the grid during the discharging process.

5.5 Case D: stabilizer design

While the operation condition for the smart charging station varies stochastically, the stabilizer is designed and attached to the smart charging station to supply additional damping torques into the system.

The stabilizer via the active and reactive power loops is designed respectively under the condition that the equivalent synchronous machine supplies 20 MW and the smart charging station consumes 10 MW of active power. A three-phase short-circuit fault happens in Bus s at 0.5 s and lasts for 0.1 s.

The forward path is:

$$\begin{cases} F_{\text{pssp}}(s) = -6.875\,1 + \text{j}6.829\,3 \\ F_{\text{pssq}}(s) = 1.7520 + \text{j}7.284\,1 \end{cases} \tag{13}$$

The parameters of the designed stabilizer attached to active and reactive power regulators, respectively, are (**Table 4**).

With the designed stabilizer, the eigenvalue of the system with the smart charging station can be obtained as that, the effectiveness of the designed stabilizers is verified by the time-domain simulation in **Figure 6** and eigenvalue calculation in **Table 5**. From **Table 5** and **Figure 6**, it can be seen that the designed stabilizer attached to the smart charging station can not only help to reduce the power fluctuations for PEV charging, but also suppress the power oscillation in the tie-line.

5.6 Case E: analysis in the four-machine power system

The power system integrated with the smart charging station is shown in **Figure 7**. The Prony method is employed to analyze the time-domain simulation of the power flow in the tie-line L6-7 [27]. The critical inter-area electromechanical

Stabilizer	Parameters
Stabilizer via active power regulator	$T_1 = T_3 = 0.019\,5$; $T_2 = T_4 = 0.5$; $K_W = 16.570\,4$
Stabilizer via reactive power regulator	$T_1 = T_3 = 0.081\,0$; $T_2 = T_4 = 0.5$; $K_W = 12.628\,9$

Table 4.
Parameters of smart charging station-based stabilizers.

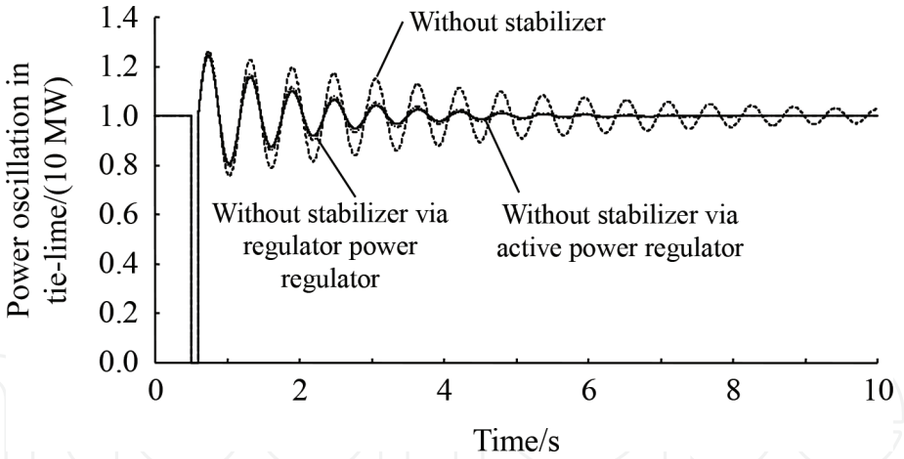

Figure 6.
Comparisons of tie-line power oscillation without and with the stabilizer via active and reactive power regulators under P_{PEV} *= 10 MW,* P_t *= 20 MW.*

Without the stabilizer	−0.241 9 + j10.864 4
With the stabilizer via active power regulator	−0.759 0 + j10.816 9
With the stabilizer via reactive power regulator	−0.651 1 + j10.847 1

Table 5.
Eigenvalue of the oscillation mode without and with stabilizers under PPEV 10 MW, Pt 20 MW.

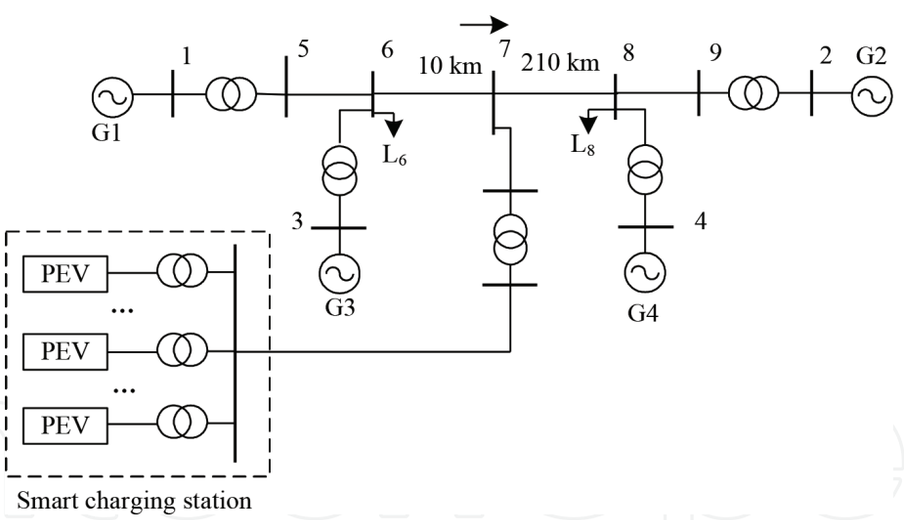

Figure 7.
Four-machine power system integrated with the smart charging station.

oscillation frequency f_{critical} and its corresponding attenuation factor α_{critical} are extracted. The eigenvalue of the critical oscillation mode is $\lambda_{\text{critical}} = \alpha_{\text{critical}} + j2\pi f_{\text{critical}}$.

With the load-flow in the tie-line $L_{6\text{-}7}$ fixed at 70 MW, a comparison is done between the proportional controlled smart charging station and the adjustable load/generator connected at Bus 7, respectively. The eigenvalue related to the inter-area oscillation mode is a concern. From **Table 6**, only the proportional controlled smart charging station functions as the adjustable load during charging period and as the regulable generator in discharging mode in view of the damping ratio.

Proportional control of the smart charging station only supplies the synchronous torque and integral control that introduces the damping torque into the grid.

P_{G2}/(10 MW)	P_{PEV}/(10 MW)	Frequency/Hz	Damping ratio/%	Adjustable load/generator*/(10 MW)	Frequency/Hz	Damping ratio/%
9.0	3.0	0.4724	3.12	3.0	0.4724	3.12
8.5	2.5	0.4710	3.14	2.5	0.4710	3.14
8.0	2.0	0.4693	3.15	2.0	0.4693	3.15
7.5	1.5	0.4672	3.16	1.5	0.4672	3.16
7.0	1.0	0.4650	3.15	1.0	0.4650	3.15
6.5	0.5	0.4624	3.13	0.5	0.4624	3.13
6.0	0.0	0.4595	3.11	0.0	0.4595	3.11
5.5	−0.5	0.4564	3.07	−0.5	0.4564	3.07
5.0	−1.0	0.4530	3.01	−1.0	0.4530	3.01

'+' denotes the adjustable load absorbing active power from the grid; '−' denotes the regulable generator injecting active power into the grid.

Table 6.
Comparison of eigenvalue related to inter-area oscillation mode only utilizing the proportional control of the smart charging station.

P_{G2}/(10 MW)	P_{PEV}/(10 MW)	Frequency/Hz	Damping ratio/%
9.0	3.0	0.4734	2.52
8.5	2.5	0.4778	2.64
8.0	2.0	0.4802	2.98
7.5	1.5	0.4753	2.56
7.0	1.0	0.4725	2.48
6.5	0.5	0.4683	2.34
6.0	0.0	0.4611	2.25
5.5	−0.5	0.4627	2.30
5.0	−1.0	0.4721	2.39

Table 7.
Comparison of eigenvalue related to the inter-area oscillation mode utilizing PI control of the smart charging station.

Conclusion (1) obtained in the single-machine infinite-busbar power system is also available in the multi-machine power system.

Both proportional and integral controls are utilized in the smart charging station. A comparison is done under different charging or discharging power capacities of the smart charging station when the load-flow in the tie-line is fixed at 70 MW. The eigenvalue related to the inter-area oscillation mode is concerned. The results are shown in **Table 7**.

From **Table 7**, the optimal charging point with the highest damping ratio in the single-machine power system can be obtained by Eq. (8) and verified by the damping torque calculation; and it also exists in the multi-machine power system. But, because of the complex interconnection of the synchronous machines and the

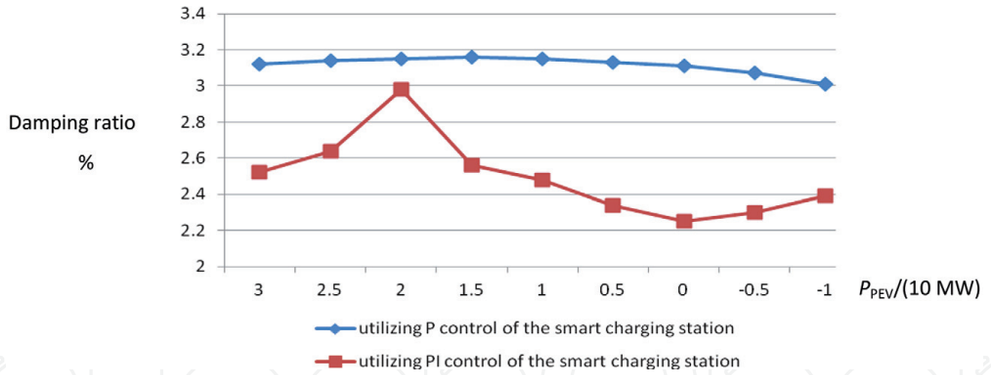

Figure 8.
Comparison of damping ratio related to inter-area oscillation mode utilizing the P and PI control of the smart charging station, respectively.

smart charging station, it is difficult to calculate the optimal charging point in theory (**Figure 8**).

6. Conclusion

The chapter investigates the impacts of a grid-connected smart charging station on power system's small-signal stability based on a simple single-machine infinite-bus power system integrated with a smart charging station. Damping torque analysis (DTA) is employed to examine the contribution from the smart charging station to the electromechanical oscillation loop of the generator in theoretical analysis. The analysis has concluded that, the smart charging station affects power system's small-signal stability in light of its interaction with the synchronous machine. The proportional controls in the smart charging station mainly induce the synchronous torque into the oscillation loop and the majority of damping torque is introduced by integral controls. The damping torque supplied by the smart charging station is mainly directly induced into the oscillation loop, and the damping torque from the excitation system is almost from the synchronous machine itself. The optimal operation condition of the smart charging station is the moment when the system has the highest damping ratio. In this chapter, such an optimal operation condition is defined, indicating that the optimal charging capacity is considered for smart charging station design.

Results of the damping torque computation of a single-machine power system integrated with a smart charging station, confirmed by eigenvalue calculations of system oscillation mode, are presented in the chapter. The conclusions obtained from the theoretical analysis are demonstrated and verified by these results. Under the optimal operation condition, the total damping torque supplied from the smart charging station and synchronous machine reaches its maximum value. During the discharging process, the damping of the system tends to deteriorate with the increasing power injected from the smart charging station to the grid. Another four-machine power system is employed to manifest that the conclusions obtained in the single-machine power system are also available in the multi-machine power system.

The stabilizer is designed and attached to the active or reactive power regulator of the smart charging station to supply additional positive damping into the system. The phase compensation method is used here. The effectiveness is confirmed by the

nonlinear simulations and eigenvalue calculations in the single-machine power system.

Although the configuration of the power system with the grid-connected smart charging station and the function to describe the charging/discharging behaviors of EVs adopted in this chapter are very simple, all the essential elements have been included to serve the purpose of study, which can thoroughly reveal the dynamic interaction between the equivalent smart charging station and conventional generation in the transmission system. The optimal charging capacity is better to be considered during the capacity design of the smart charging station. With the help of the designed smart charging station-based stabilizer, the small-signal stability can be effectively maintained. Studies on the interactions among several smart charging stations with the dynamic stability in distribution systems and the uncertainties and diversities of EV charging/discharging behaviors will be carried out for future researches.

A. Appendix: the parameters of example systems

1. Single-machine infinite-busbar power system.

The parameters of the synchronous machine (The unit is in pu):
$M = 5.0$; $T'_{d0} = 5.0$ s; $D = 1.2$; $X_d = 0.8$; $X_q = 0.4$; $X'_d = 0.05$; $\omega_0 = 2 \times 50\pi$;
$U_{\mathrm{t}} = 1.05$; $U_{\mathrm{tref}} = 1.05$; $K_{\mathrm{a}} = 20.0$; $T_{\mathrm{a}} = 0.01$ s.
The parameters of the network (The unit is in pu): $X_{\mathrm{ts}} = 0.2$; $X_{\mathrm{sb}} = 0.1$;
$X_{\mathrm{s}} = 0.1$; $U_{\mathrm{b}} = 1.0$.
The parameters for the smart charging station(The unit is in pu):
$K_{\mathrm{PP}} = 20$, $K_{\mathrm{IP}} = 20$, $K_{\mathrm{PI}_q} = 0.3$, $K_{\mathrm{II}_q} = 0.3$, $K_{\mathrm{PQ}} = 15$, $K_{\mathrm{IQ}} = 15$, $K_{\mathrm{PI}_d} = 0.7$,
$K_{\mathrm{II}_d} = 0.7$.

2. Four-machine power system.

The parameters of the synchronous machine are:
$T_{\mathrm{J1}} = T_{\mathrm{J2}} = 117$; $T_{\mathrm{J3}} = T_{\mathrm{J4}} = 111.15$; $T'_{d01} = T'_{d02} = T'_{d03} = T'_{d04} = 8.0$ s;
$D_{\mathrm{mac1}} = D_{\mathrm{mac2}} = D_{\mathrm{mac3}} = D_{\mathrm{mac4}} = 5.0$ pu; $X_{d1} = X_{d2} = X_{d3} = X_{d4} = 0.2$;
$X_{q1} = X_{q2} = X_{q3} = X_{q4} = 0.1889$; $X'_{d1} = X'_{d2} = X'_{d3} = X'_{d4} = 0.0333$;
$\omega_{01} = \omega_{02} = \omega_{03} = \omega_{04} = 100\pi$; $U_{\mathrm{t1}} = U_{\mathrm{t3}} = 1.03$; $U_{\mathrm{t2}} = U_{\mathrm{t4}} = 1.01$;
$U_{\mathrm{tref1}} = U_{\mathrm{tref3}} = 1.03$; $U_{\mathrm{tref2}} = U_{\mathrm{tref4}} = 1.01$.
All the generators are equipped with the same AVR: $K_{\mathrm{a}} = 50$; $T_{\mathrm{a}} = 0.55$ s;
The parameters of the smart charging station are (in pu):
$K_{\mathrm{PP}} = 20$, $K_{\mathrm{IP}} = 20$, $K_{\mathrm{PI}_q} = 0.3$, $K_{\mathrm{II}_q} = 0.3$;
$K_{\mathrm{PQ}} = 15$, $K_{\mathrm{IQ}} = 15$, $K_{\mathrm{PI}_d} = 0.7$, $K_{\mathrm{II}_d} = 0.7$.
The parameters of the lines are (in pu): $X_{15} = X_{36} = X_{29} = X_{48} = 0.01667$;
$X_{56} = X_{89} = 0.025$; $X_{67} = 0.105$; $X_{78} = 0.005$.

G1 is connected with the slack bus of the system.G3 and G4 generate 70 MW of active power, respectively. The loads at Bus 6 and Bus 8 are 100 and 200 MW accordingly.

Acknowledgements

The authors would like to acknowledge the support of Dr. Tim Littler from Queen's University, Belfast, UK.

DOI: http://dx.doi.org/10.5772/intechopen.80721

Author details

Cai Hui
State Grid Jiangsu Economic Research Institute, Nanjing, P.R. China

*Address all correspondence to: caihui300@hotmail.com

References

[1] Zhenya L. Electric Power and Energy in China. Beijing: China Electric Power Press; 2012. pp. 124-135 (in Chinese). ISBN: 978-7-5123-2667-5

[2] Zheng J, Mehndiratta S, Guo JY, et al. Strategic policies and demonstration program of electric vehicle in China. Transport Policy. 2012;**19**(1):17-25. DOI: 10.1016/j.tranpol.2011.07.006

[3] Bowen Z, Littler T. Local storage meets local demand: A technical solution to future power distribution system. IET Generation, Transmission and Distribution. 2016;**10**(3):704-711. DOI: 10.1049/iet-gtd.2015.0442

[4] Venayagamoorthy GK. SmartParks for short term power flow control in smart grids. In: IEEE International Electric Vehicle Conference (IEVC) 2012. Greenville, USA: IEEE; 2012. pp. 1-6. DOI: 10.1109/IEVC.2012.6183288

[5] Mitra P, Venayagamoorthy GK. SmartPark as a virtual STATCOM. IEEE Transactions on Smart Grid. 2011;**2**(3):445-455. DOI: 10.1109/TSG.2011.2158330

[6] Mitra P, Venayagamoorthy GK. Intelligent coordinated control of a wind farm and distributed SmartParks. In: IEEE Industry Application Society Annual Meeting (IAS) 2010. Houston, USA: IEEE; 2010. pp. 1-8. DOI: 10.1109/IAS.2010.5615930

[7] Tomic J, Kempton W. Using fleets of electric drive vehicles for grid support. Journal of Power Sources. 2007;**168**(2):459-468. DOI: 10.1016/j.jpowsour.2007.03.010

[8] Venayagamoorthy GK, Sharma RK, Gautam PK. Dynamic energy management system for a smart microgrid. IEEE Transactions on Neural Networks and Learning Systems. 2016;**27**(8):1643-1656. DOI: 10.1109/TNNLS.2016.2514358

[9] Kempton W, Tomic J. Vehicle-to-grid power fundamentals: Calculating capacity and net revenue. Journal of Power Sources. 2005;**144**(1):268-279. DOI: 10.1016/j.jpowsour.2004.12.025

[10] Xifan W, Chengcheng S, Xiuli W, et al. Survey of electric vehicle charging load and dispatch control strategy. Proceedings of the CSEE. 2013;**33**(1):1-10 (in Chinese). Available from: http://d.wanfangdata.com.cn/Periodical/zgdjgcxb201301001

[11] Kempton W, Tomic J. Vehicle-to-grid power implementation: From stabilizing the grid to support large-scale renewable energy. Journal of Power Sources. 2005;**144**(1):280-294. DOI: 10.1016/j.jpowsour.2004.12.022

[12] Liting T, Mingxia Z, Wang H. Evaluation and solutions for electric vehicles' impact on the grid. Proceedings of the CSEE. 2012;**32**(31):43-49 (in Chinese). Available from: http://d.wanfangdata.com.cn/Periodical/zgdjgcxb201231006

[13] Huston C, Venayagamoorthy GK, Corzine K. Intelligent scheduling of hybrid and electric vehicle storage capacity in a parking lot for profit maximization in grid power transaction. In: Proceedings of IEEE Energy 2030. Atlanta, USA: IEEE; 2008. pp. 1-8. DOI: 10.1109/ENERGY.2008.4781051

[14] Zhengshuo L, Hongbin S, Guo Q, et al. Study on wind-EV complementation on the transmission grid side considering carbon emission. Proceedings of the CSEE. 2012;**32**(10):41-48 (in Chinese). Availabe from:

http://explore.bl.uk/primo_library/libweb/action/display.do?tabs=detailsTab&gathStatTab=true&ct=display&fn=search&doc=ETOCRN613373549&indx=1&recIds=ETOCRN313900056

[15] Xiaoyan Y, Chunlin G, Xuan X, Dequan H, Zhou M. Research on large scale electric vehicles participating in the economic dispatch of wind and thermal power system. In: 2017 China International Electrical and Energy Conference. 2017. pp. 223-228. DOI: 10.1109/CIEEC.2017.8388450

[16] Hua P, Zuofang L, Qianzhong X. Economic dispatch of power system including electric vehicle and wind farm. In: 2017 IEEE Conference on Energy Internet and Energy System Integration. 2017. pp. 1-5. DOI: 10.1109/EI2.2017.8245238

[17] Beck LJ. V2G—101, a text about vehicle-to-grid (V2G), the technology which enables a future of clean and efficient electric-powered transportation. USA:V2G-101 Copyright; 2009. pp. 10-25

[18] Yaonan Y. Electric Power System Dynamics. New York: Academic Press; 1983. pp. 79-94. ISBN: 0127748202

[19] Wenjuan D, Haifeng W, Jun C. Model and theory of PSS localized phase compensation method. Proceeding of the CSEE. 2012;**32**(19):36-41 (in Chinese)

[20] Wenjuan D, Haifeng W, Jun C. Application of localized phase compensation method to design a stabilizer in a multi-machine power system. Proceeding of the CSEE. 2012; **32**(22):73-78 (in Chinese). Available from: http://explore.bl.uk/primo_library/libweb/action/display.do?tabs=detailsTab&gathStatTab=true&ct=display&fn=search&doc=ETOCRN613373549&indx=1&recIds=ETOCRN320143870

[21] Lingling Y, Wenjuan D, Yizhang Y, Yanfeng G. Methods of DTA to estimate the impact of integration of DFIG on single-machine infinite-bus power system. In: 2016 China International Conference on Electricity Distribution. 2016. pp. 1-5. DOI: 10.1109/CICED.2016.7576247

[22] Wenjuan D, Haifeng W, Liye X. Power system small-signal stability as affected by grid-connected photovoltaic generation. European Transactions on Electrical Power. 2012; **22**(5):688-703

[23] Wenjuan D, Haifeng W, Hui C. Modeling a Grid-connected SOFC power plant into power systems for small-signal analysis and control. European Transactions on Electrical Power. 2012;**23**(3):330-341. DOI: 10.1049/cp.2011.0208

[24] Haifeng W, Swift FJ. The capability of the static var compensator in damping power system oscillations. IEE Proceedings of Generation, Transmission and Distribution. 1996; **143**(4):353-358 Availabe from: https://explore-bl-uk.vpn.seu.edu.cn/primo_library/libweb/action/display.do?tabs=detailsTab&gathStatTab=true&ct=display&fn=search&doc=ETOCRN613373549&indx=1&recIds=ETOCRN011774271

[25] Majeau-Bettez G, Hawkins TR, Stroemman AH. Life-cycle environmental assessment of lithium-ion and nickel metal hydride batteries for plug-in hybrid and battery electric vehicles. Environmental Science and Technology. 2011;**45**(10):4548-4554

[26] Stikes K, Gross T, Lin Z, et al. Plug-in Hybrid Electric Vehicle Market Introduction Study: Final Report.

Washington, DC: Tech. Rep. DE2010-972306; 2010

[27] Guoqiang H, Renmu H, Huachun Y, et al. Iterative prony method based power system low frequency oscillation mode analysis and PSS design. In: 2005 IEEE/PES Asia and Pacific Transmission and Distribution Conference and Exhibition. Dalian, China: IEEE; 2005. pp. 1-6. DOI: 10.1109/TDC.2005.1546867